Work function and quantum efficiency study of metal oxide thin films on Ag(100)

V. Chang,[1] T. C. Q. Noakes,[2] and N. M. Harrison[3,*]

[1]*Department of Materials, Imperial College London, South Kensington, London, SW7 2AZ, United Kingdom*

[2]*Daresbury Laboratory, Daresbury, Warrington, WA4 4AD, United Kingdom*

[3]*Department of Chemistry, Imperial College London, South Kensington, London, SW7 2AZ, United Kingdom*

(Received 27 February 2018; published 30 April 2018)

Increasing the quantum efficiency (QE) of metal photocathodes is in the design and development of photocathodes for free-electron laser applications. The growth of metal oxide thin films on certain metal surfaces has previously been shown to reduce the work function (WF). Using a photoemission model B. Camino *et al.* [Comput. Mater. Sci. **122**, 331 (2016)] based on the three-step model combined with density functional theory calculations we predict that the growth of a finite number of MgO(100) or BaO(100) layers on the Ag(100) surface increases significantly the QE compared with the clean Ag(100) surface for a photon energy of 4.7 eV. Different mechanisms for affecting the QE are identified for the different metal oxide thin films. The addition of MgO(100) increases the QE due to the reduction of the WF and the direct excitation of electrons from the Ag surface to the MgO conduction band. For BaO(100) thin films, an additional mechanism is in operation as the oxide film also photoemits at this energy. We also note that a significant increase in the QE for photons with an energy of a few eV above the WF is achieved due to an increase in the inelastic mean-free path of the electrons.

DOI: 10.1103/PhysRevB.97.155436

I. INTRODUCTION

Free-electron lasers (FELs) are coherent light sources that produce tuneable radiation from x-rays to THz in pulses on the femtosecond timescale [1]. These properties make FELs the state of the art for the study of ultrafast processes with atomic resolution [2]. The lasing medium in a FEL are free electrons that are produced by the photoelectric effect from a photocathode. The development of a high quantum efficiency (QE), high durability, low emittance, and fast response photocathode is crucial for the improvement and development of FELs [3].

Metals are used as photocathodes because of their durability and fast response time. However, they usually have a high work function (WF) that limits the QE, which is defined as the proportion of electrons emitted per incident photon. The typical QE in photocathode metals such as Cu or Ag is on the order of 10^{-5}, which is much lower than the typical QE of semiconductors (10^{-2}) [3]. One way to improve the QE of a metal photocathode is through the reduction of the WF. Change of the metal-surface WF can be achieved by the adsorption of atomic species that change the surface dipole [4]. The adsorption of atomic species also has the potential to induce changes in the surface band structure and therefore to change the photoemission properties of the surface [5].

Previous experimental and theoretical works [6–9] have shown that the addition of metal oxide thin films on specific surfaces of metals such as the (100) surface of face center cubic (fcc) metals produces a surface with a lower WF. Goniakowski and Noguera identify three distinct mechanisms for the WF changes (charge transfer, electrostatic compression, and surface reconstruction) [10]. In particular, the epitaxial growth of MgO thin films on Ag(100) has been widely studied in both experimental [11] and theoretical works [12,13], and a significant reduction in the Ag(100) surface WF of more than 1 eV by the addition of 1 to 12 atomic layers of MgO is both computed and observed. The QE of a 4-MgO-layer film on Ag(100) has also been studied and for a photon energy of 4.66 eV the QE is seven times higher than that of the clean metal surface [14].

Metal oxides, such as MgO, are chemically stable and could be able to protect the clean metal surface from oxidation, which is often the cause of photocathode degradation. The direct oxidation of the photocathode and the adsorption of oxygen affects the performance of the photocathode by lowering the QE. To avoid this problem, photocathodes are usually operated under ultrahigh-vacuum conditions [15].

Because metal oxide thin films have the potential to improve the QE and chemical stability, surface engineering of films on metal photocathodes is a promising way to develop a new generation of efficient and stable photocathodes.

II. COMPUTATIONAL DETAILS

Density functional theory (DFT) calculations using a plane-wave (PW) basis set were carried out using CASTEP 8.0. Core electrons were replaced by ultrasoft pseudopotentials generated on the fly by CASTEP [16]. The effects of electronic exchange and correlation are approximated by using the PBEsol generalized gradient approximation (GGA) density functional [17]. A variation in the total electronic energy per atom on the order of 10^{-5} eV was found for a plane wave cutoff energy of 750 eV and a Monkhorst–Pack sampling of the Brillouin zone (BZ) of $16 \times 16 \times 16$ forthe bulk and $16 \times 16 \times 1$ for the slabs [18].

The Ag, MgO, and BaO structures are based on the fcc Bravais lattice (space group 225). Simulations of the bulk

*nicholas.harrison@imperial.ac.uk

TABLE I. Computed WF, WF reduction, interplanar distance d between MgO thin film and Ag(100) surface, and the formation energy of the metal oxide thin film computed by using PBEsol for two different registries where Mg atoms atop Ag atoms (Mg-Top) and when O atoms are atop of Ag atoms (O-Top). The experimental measurements of the WF of MgO thin films on Ag(100) surface and the scanning tunneling microcopy measurements of the metal-oxide-metal substrate distance are also presented.

	ML	Φ (eV)	$\Delta\Phi$ (eV)	d (Å)	Formation energy (J/m^2)
Mg-Top	1	3.88	−0.43	3.16	1.67
	2	3.65	−0.66	3.65	1.77
	3	3.76	−0.55	3.22	1.85
O-Top	1	3.15	−1.16	2.56	1.10
	2	2.82	−1.49	2.62	1.30
	3	2.84	−1.47	2.59	1.38
Expt.	1		−1.2[a]	2.39–2.55[b]	
	2			2.46–2.55[b]	
	3		−1.4[a]		

[a]Reference [11].
[b]Reference [6].

structures predict a lattice parameter of 4.064 Å for Ag, 4.241 Å for MgO, and 5.561 Å for BaO (experimental lattice parameters are 4.0853 Å [19], 4.212 Å [20], and 5.539 Å [21], respectively). The Ag(100) surface is simulated using a three-dimensional (3D) periodic slab model with a vacuum gap of at least 20 Å and a thickness of 10 atomic layers. The displacement upon relaxation of atoms in the center of the slab is found to be less than 0.2% of the bulk interplanar distance. The surface energy of Ag(100) is found to be 1.080 J/m^2, which is in good agreement with previous theoretical DFT calculations within the PBE approximation for electronic exchange and correlation [22]. The WF is approximated as the difference between the Fermi energy and the constant value of the electrostatic potential at the center of the vacuum region of the 3D periodic slab model. The formation energy of the metal oxide thin films is calculated as

$$E_{\text{Slab}} = E_{\text{Tot}} - E_{\text{Ag(100)}} - nE_{\text{MO}_{\text{bulk}}}, \quad (1)$$

where E_{Slab} is the energy required to form the metal oxide thin film relative to the bulk oxide, E_{Tot} is the computed total energy of the system, $E_{\text{Ag(100)}}$ is the computed energy of the Ag slab, $E_{\text{MO}_{\text{bulk}}}$ is the computed energy for the bulk metal oxide per formula unit, and n is the number of formula units of oxide per unit cell of the slab model.

A photoemission model [4] is used to study the quantum efficiency and photoemission properties of the metal oxide thin films on metal substrates. This model, which is based on Spicer's three-step model [23], facilitates the decomposition of the quantum efficiency into contributions from each atomic layer in the slab model. The transport of the photoexcited electrons to the surface is described based on an estimated, energy-dependent, inelastic mean-free path (IMFP). The IMFP for Ag used in this work is obtained by averaging values found in the literature [4,24,25]. In the current work, the IMFP in the oxide film is approximated by that of the metal substrate. For an electron with an energy of 4.7 eV above the Fermi energy, the IMFP is thus approximated as 6.13 Å.

III. RESULTS AND DISCUSSION

A. MgO/Ag(100)

There is a small lattice mismatch between Ag (4.085 Å) and MgO (4.212 Å) and 1×1 MgO(100) layers can be grown epitaxially on the Ag(100) surface [6,26]. There are two likely registries at the interface, either with O atoms atop Ag atoms (O-Top) or Mg atoms atop Ag atoms (Mg-Top), both of which are found to be local minima. The registry of MgO/Ag(100) is studied for 13 monolayers (MLs) of MgO. The computed formation energy, MgO-Ag distance d, WF Φ, and WF difference $\Delta\Phi$ for the two different surface registries are presented in Table I.

The lower formation energy of O-Top suggests that MgO thin films will growth epitaxially on the Ag(100) surface in this registry. Scanning tunneling microscopy STM measurements

TABLE II. Computed WF, WF reduction and QE for MgO thin films on Ag(100) surface and the clean Ag(100) surface using PBEsol. Previous theoretical using PW91 and experimental results of the WF and WF reduction are also presented in this table. The computed values presented in this work shows good agreement with previous studies.

		Present			Previous calculations[a]		Experimental[b]	
	NL	Φ (eV)	$\Delta\Phi$ (eV)	QE (4.7 eV) (el./phot.)	Φ (eV)	$\Delta\Phi$ (eV)	Φ (eV)	$\Delta\Phi$ (eV)
Ag(100)		4.31		1.4×10^{-5}	4.23		4.64	
MgO/Ag(100)	1	3.15	−1.16	7.5×10^{-4}	3.34	−0.94		−1.2
	2	2.82	−1.49	4.6×10^{-4}	2.95	−1.28		
	3	2.84	−1.47	2.9×10^{-4}	2.96	−1.27		−1.4
	4	2.75	−1.56	1.8×10^{-4}				
	5	2.66	−1.65	9.7×10^{-5}				
	6	2.71	−1.60	2.5×10^{-5}				
	7	2.71	−1.60	4.1×10^{-5}				
	8	2.72	−1.59	2.7×10^{-5}				−1.3

[a]Reference [9].
[b]Reference [11].

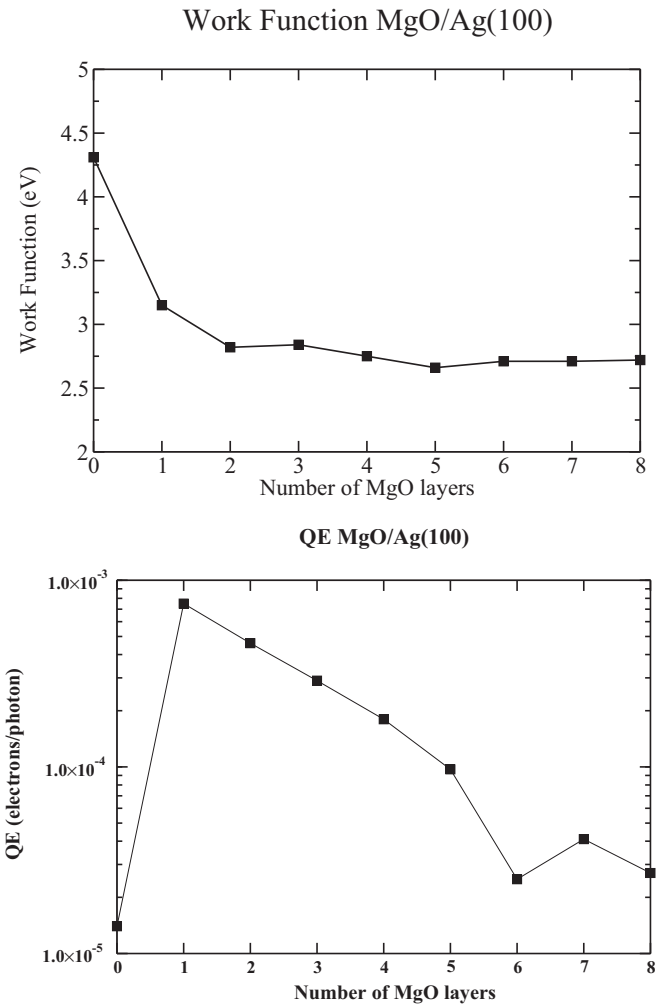

FIG. 1. Variation of the (top) WF and (bottom) QE with the number of MgO layers on Ag(100) for the O-Top registry. The addition of more than two layers does not produce a significant reduction of the WF. The QE is maximize for a MgO monolayer and the addition of MgO layers lowers the QE.

of MgO monolayers grown epitaxially on Ag(100) suggest that the distance between the MgO and Ag layers is 2.39–2.55 Å [6], which is in good agreement with that computed for the O-Top configuration (2.56 Å). The WF calculated in this work, in previous calculations, and in experimental measurements are reported in Table II for MgO thicknesses up to 8 MLs, along with the computed QE for a photon energy of 4.7 eV.

The WF of the clean Ag(100) surface computed in this work is 4.31 eV, which is in reasonable agreement with previous experimental values (4.64 eV) for Ag(100) [27]. Previous experimental studies of the WF of MgO grown epitaxially on Ag(100) demonstrate a reduction of more than 1 eV for MgO films with a thickness between 1 and 12 MLs independent of the thickness of the film [7,11] Previous DFT calculations of 1–3 ML of MgO on Ag(100) computed by Pacchioni *et al.* suggest a WF reduction of between 0.94 and 1.27 eV [9]. The small discrepancy with WF values computed here is likely to be due to the use of a different GGA functional (PW91 in previous calculations and PBEsol used in this work). The WF

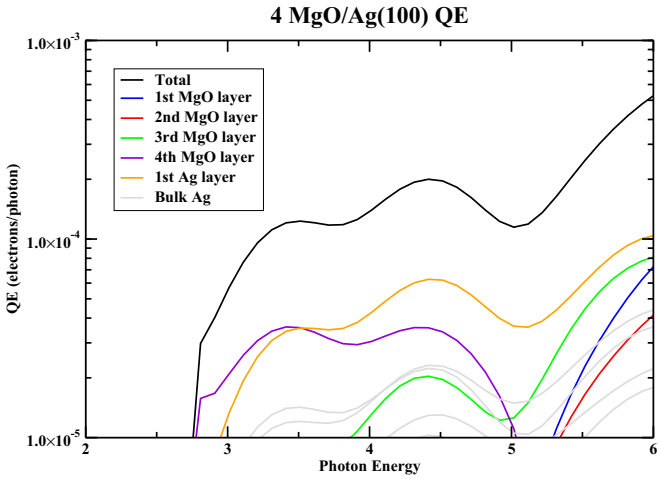

FIG. 2. Layer-by-layer decomposition of contributions to the photoemission of four MgO/Ag(100) for the O-Top registry. The first layer refers to the external MgO layer while the fourth layer is the layer at the interface between Ag and MgO. The contribution to the QE is mainly from the layers at the interface between MgO and Ag for an incident photon with an energy of 4.7 eV. For this energy, the emission of electrons from the first MgO layer, which is the layer at the surface of the system, is negligible.

reduction mechanism for MgO(100) thin films on Ag(100) has been attributed to a strong electrostatic compressive effect that modifies the surface dipole with a minor contribution from a charge-transfer mechanism due to the chemical interaction between the MgO thin film and Ag [9]. A WF reduction of between 1.16 and 1.60 eV for the MgO(100) thin films on Ag(100) in the O-Top registry for systems with 1–8 (MLs) of MgO(100) is calculated here, which is consistent with previous experimental and theoretical studies [7,9,11].

For the O-Top registry, Fig. 1 shows the variation of the computed WF and the QE at a photon energy of 4.7 eV with the number of MgO layers (1–8 MLs) on the Ag(100) surface. The addition of a finite number of MgO layers (1–5MLs) on Ag(100) is predicted to increase the QE relative to the metal substrate by two orders of magnitude for a single MgO monolayer and one order of magnitude for five MgO layers. The results of these calculations are in good agreement with an experimental measurement of four MgO layers growth on Ag(100), where the QE was found to be seven times higher than that of the clean Ag(100) [14,28]. It is notable that the addition of more layers (6–8) continues to reduce the WF but does not produce any further change in the QE. This can be understood from the decomposition of the the total photoemission into contributions from each atomic layer shown in Fig. 2. For a photon energy of 4.7 eV, the main contribution to the photoemission of electrons is produced by the first Ag layer and the fourth MgO layer, which are the layers at the metal oxide/metal interface. The total density of states (DOS), projected density of states (PDOS) on the atoms, and the band structure for clean Ag(100) and a system with four MgO layers in the O-Top registry are shown in Fig. 3. The band structure and the PDOS suggest that there is no formation of additional bands near the Fermi level that could contribute to the photoemission. The high contribution from

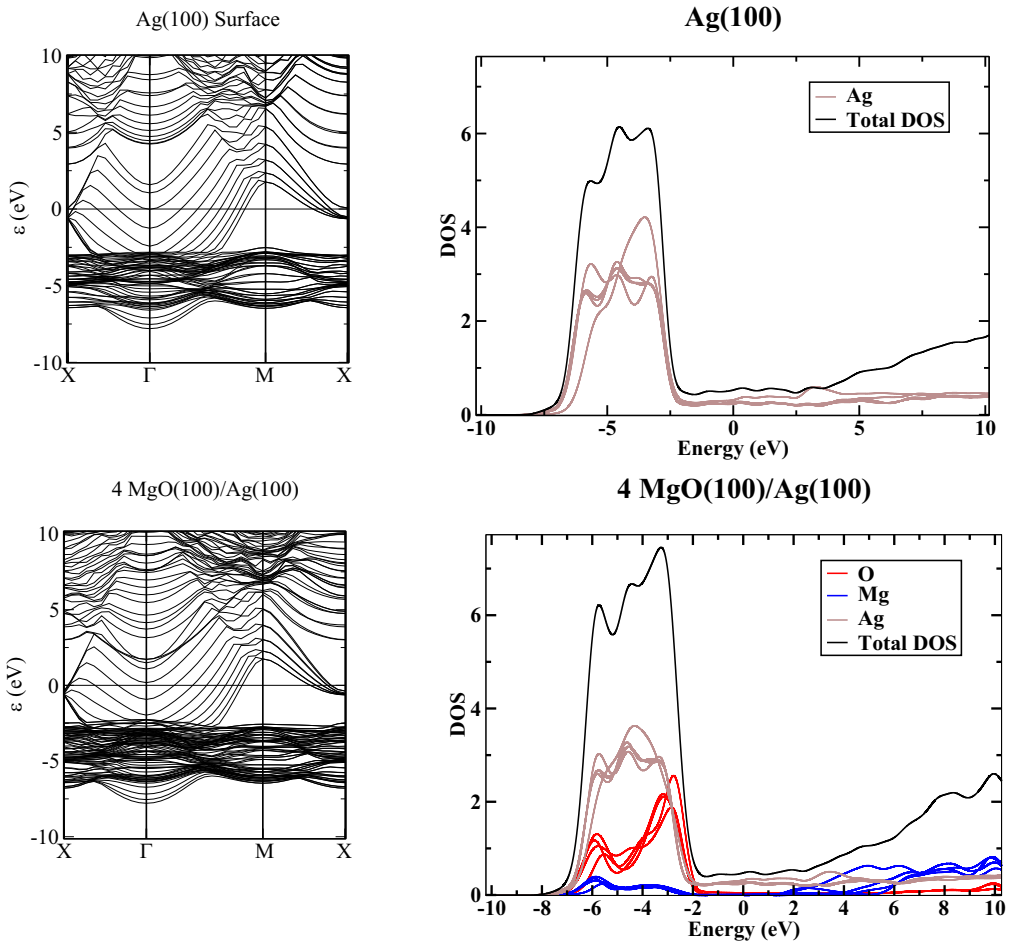

FIG. 3. Computed density of states and band structure of Ag(100) surface and for 4 MgO/Ag(100) for the O-Top registry. The projection on the different atomic species is also computed. The energy is relative to the Fermi energy. The band structure does not show a formation of additional bands near the Fermi energy. The valence band of MgO is localized at energies far below the Fermi energy and therefore electrons cannot be emitted. Charge-transfer excitation of electrons from the Ag valence band to empty MgO conduction bands is responsible for the high contribution of the interface MgO layers.

the interface MgO layers to the QE (1.8×10^{-5} from the third and 3.0×10^{-5} from the fourth layer in Fig. 2) is in fact due to the charge-transfer excitation of electrons direct from the Ag valence band to the MgO conduction bands.

Previous calculations, based on DFT-D2, have shown that the inclusion of dispersion forces between the metal oxide thin film and the metal substrate reduces the MgO-Ag distance by a few tenths of an Å and produces a shift of a few meV in the WF [29]. Reducing the MgO-Ag distance by 0.1 Å produces a reduction of 0.2 eV in the WF compared with the fully relaxed structure computed here for 3 MgO layers on Ag(100). We estimate that this produces an increase of 10% in the QE.

B. BaO/Ag(100)

The growth of BaO thin films on Ag(100) has been demonstrated by Hess *et al.* by using molecular beam epitaxy [30]. Even so, BaO thin films are potentially unstable in the presence of oxygen, which leads to the formation of BaO_2 [31,32].

Epitaxial growth of BaO on Ag(100) is not possible in the (1×1) periodicity since the BaO lattice parameter (5.539 Å) is much larger that of Ag (4.085 Å). Nevertheless, epitaxial growth is possible within a supercell periodicity. The $(\sqrt{2} \times \sqrt{2})$R45 supercell of Ag(100) has a mismatch of only 4.3% with the (1×1) BaO(100) cell. In the presented calculations, the BaO lattice constant is expanded to fit the Ag $\sqrt{2} \times \sqrt{2}$)R45 cell. Unlike MgO, where two locally stable structures are found with either O or Mg atoms sitting atop Ag atoms, in this periodicity BaO grows in the registry with both Ba and O atoms atop Ag atoms (BaO-Top) or with both Ba and O atoms in the threefold hollow sites of the Ag(100) surface (BaO-Hollow) as displayed in Fig. 4. In our calculations, we

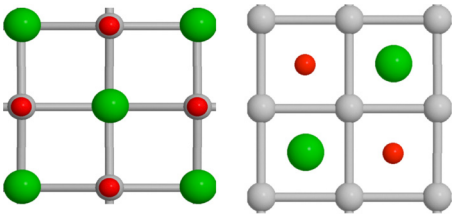

FIG. 4. (left) BaO-Top. (right) BaO-Hollow. O (red), Ba (green), and Ag (gray).

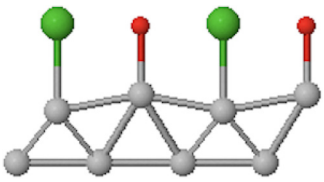

FIG. 5. Rumpling of Ag(100) surface is found after a structural relaxation study. The strong chemical interaction between Ag and BaO thin films induce a rumpling of Ag surface. O(red), Ba (green), and Ag (gray).

found that the BaO-Top structure is a locally stable structure independent of the number of adsorbed monolayers while the BaO-Hollow structure is only found to be locally stable for bilayer adsorption, otherwise it relaxes to the BaO-Top structure.

The BaO-Top structure induces a rumpling of the Ag(100) substrate, as displayed in Fig. 5. The rumpling is found to be negligible for bilayer adsorption and the computed distance between BaO thin films and the Ag(100) substrate after

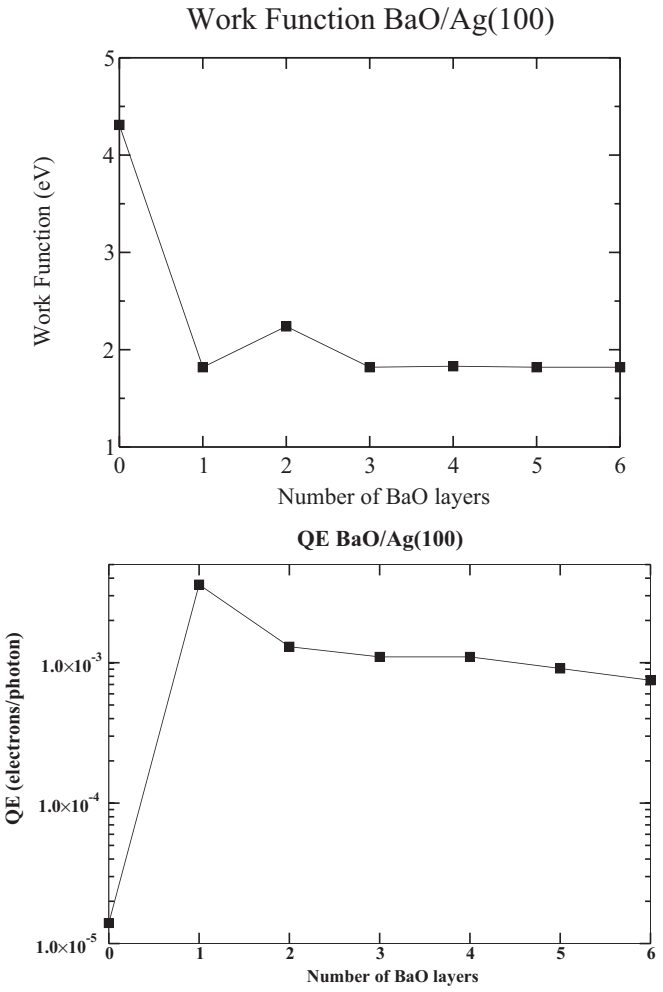

FIG. 6. Variation of the computed WF and QE with the number of BaO layers on Ag(100). The addition of more than a monolayer does not produce a significant additional reduction of the WF. The QE is maximized for a BaO monolayer and the addition of further BaO layers slightly decreases the QE.

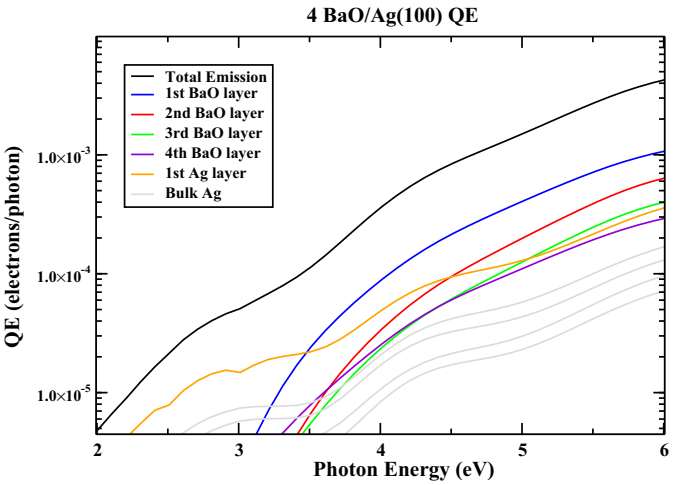

FIG. 7. Layer-by-layer decomposition of the photoemission of the 4 BaO/Ag(100) system. The first layer is referred to as the external BaO layer while the fourth layer is the layer at the interface between Ag and BaO. The main contribution to the QE is from the surface BaO layer.

relaxation of the system is 2.36 Å for a monolayer, 2.93 Å for bilayers, and 2.48 Å for trilayers. The longer distance of BaO bilayers compared with monolayers or trilayers suggest a weaker chemical interaction. This is supported by previous calculations where the charge transfer is predicted to be smaller for BaO-Top bilayers than that of the monolayers or trilayers [9]. The computed WF, formation energy, and QE for a normal incident photon with an energy of 4.7 eV and previous WF calculations and experimental measurements for the BaO-Top structure are shown in Table III.

The WF reduction calculated in this work is consistent with that calculated in previous work. The small discrepancies between previous calculations and the calculations presented here are mainly attributed to the use of a different GGA functional used. Pacchioni described the WF reduction mechanism as a combination of the electrostatic compressive effect and charge transfer due to the strong chemical interaction between the BaO thin film and Ag [9]. UPS measurements of a BaO monolayer on Ag(100) show a significant WF reduction of 1.74 eV [30]. As expected, the reduction in WF results in a strong increase in the computed QE, which is 250 times larger than that computed for the clean Ag(100) surface. Figure 6 shows the QE for a photon energy of 4.7 eV and WF reduction by the addition of 1–6 MLs of BaO on Ag(100). As in the MgO/Ag(100) case, the initial QE improvement decays as more layers of BaO are added. This is due to the inelastic scatterings of excited electrons exiting from the Ag substrate. However, this QE reduction is smaller in magnitude than that computed for the MgO/Ag(100) case, where after the addition of six or more layers, the QE improvement over the bare metal is negligible. The layer-by-layer decomposition of the system of four BaO(100) layers on Ag (100) is displayed in Fig. 7 and shows that, as this film thickness is achieved, the main contribution to the emission of electrons is from photoexcitations within the BaO film rather than the Ag substrate. Previous photoemission studies of BaO surfaces [33] suggest that the

TABLE III. Computed WF, WF reduction, and QE for BaO thin films on Ag(100) surface and the clean Ag(100) surface using PBEsol. Previous calculations using PW91 and experimental results of the WF and WF reduction are also presented. The values computed here are in good agreement with previous studies.

		Present			Previous calculations[a]		Experimental[b]	
	NL	Φ (eV)	ΔΦ (eV)	QE (4.7 eV) (el./phot.)	Φ (eV)	ΔΦ (eV)	Φ (eV)	ΔΦ (eV)
Ag(100)		4.31		1.4×10^{-5}	4.23		4.24	
BaO/Ag(100)	1	1.82	−2.49	3.6×10^{-3}	1.91	−2.31	2.5	−1.74
	2	2.24	−2.07	1.3×10^{-3}	2.53	−1.70		
	3	1.82	−2.49	1.1×10^{-3}	2.03	−2.20		
	4	1.83	−2.48	1.1×10^{-3}				
	5	1.82	−2.49	9.1×10^{-4}				
	6	1.82	−2.49	7.5×10^{-4}				

[a]Reference [9].
[b]Reference [30].

QE for photoemission from BaO for a photon energy of 4.7 eV is of the order of 10^{-5}, which is similar to that observed in metals such as Cu or Ag. The relatively small band gap of BaO (4.10 eV [34]) compared with other metal oxides, such as MgO (7.8 eV [34]), allows electrons to be excited by 4.7 eV photons to bands above the vacuum level and to be emitted.

The BaO-Hollow structure is only found to be a local energy minimum in structure relaxation for bilayer adsorption. The WF, the QE for a normal incident photon with an energy of 4.7 eV, and the formation energy of the BaO-Hollow bilayer and BaO-Top bilayer are shown in Table IV. The BaO-Hollow bilayer shows a higher QE than BaO-Top bilayers despite its higher WF. The DOS displayed in Fig. 8 shows that the BaO-Hollow bilayer valence band is closer in energy to the Fermi energy and this increases significantly the number of states near the Fermi energy. The photoemission from these states enhances the QE. Even so, it is the adsorption of a system with a BaO monolayer in the BaO-Top registry that yields the highest QE and the addition of a higher number of layers does not produce any further increment of the QE.

UPS measurements of BaO adsorbed to Ag(100) at 1 ML coverage have been interpreted in terms of two distinct surface phases: a majority phase with a WF of 2.5 eV and a minority phase with a WF of 2.8 eV. In both cases, XPS measurements suggest negligible charge transfer [30]. The results presented here suggest a different interpretation. It is possible that, in those experiments, BaO bilayers had been formed rather than monolayers. The current results suggest that only bilayers

TABLE IV. Computed WF, WF reduction, and QE for BaO bilayers on Ag(100). Two different structures are computed: when BaO atoms are sitting on the top of Ag atoms (BaO-Top) and when BaO atoms are sitting on the hollows of Ag(100) surface. Despite the WF reduction, the BaO-Hollow registry shows a higher QE.

		Φ (eV)	ΔΦ (eV)	QE (4.7 eV) (el./phot.)	Formation energy (J/m^2)
Ag(100)		4.31		1.4×10^{-5}	
BaO/Ag(100)	Hollow	2.79	−1.52	2.6×10^{-3}	0.630
	Top	2.24	−2.07	1.3×10^{-3}	0.540

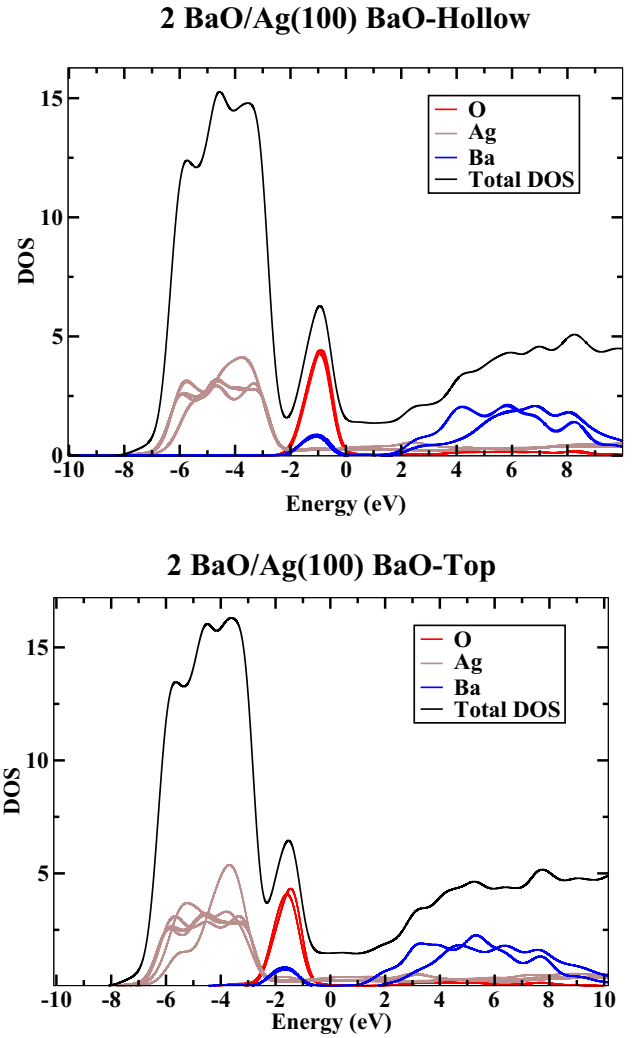

FIG. 8. Computed density of states (top) of BaO bilayer when BaO atoms are sitting on the hollow of Ag(100) surface (BaO-Hollow). Computed density of states (bottom) of BaO bilayer when BaO atoms are sitting on the top of Ag atoms (BaO-Top). The computed density of states suggests a higher number of states around the Fermi level ($E_{\text{Fermi}} = 0$ eV) in the BaO-Hollow that might be responsible for the higher QE of this registry.

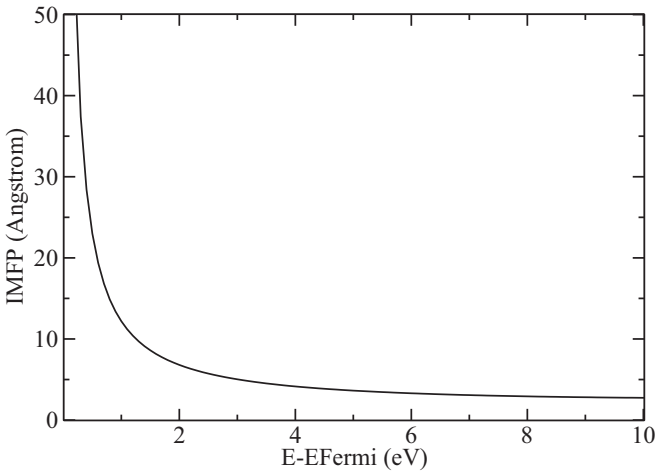

FIG. 9. Computed inelastic mean-free path for Ag using the formalism of Ref. [24]. The universal curve suggests that electrons with energies within 2 eV to the Fermi energy have significantly longer mean-free paths than those at higher energies.

can be grown with two different registries (BaO-Top and BaO-Hollow structures). The computed formation energy of BaO-Top and BaO-Hollow adsorbed bilayers (0.540 J/m^2 and 0.630 J/m^2, respectively) are similar and lower than that of the BaO-Top monolayer (0.784 J/m^2). It is therefore possible that both bilayer registries were formed in the experiment. This model is supported by the fact that the computed WF presented here (2.24 and 2.79 eV) are also in agreement with the measured WF for the two observed phases (2.5 and 2.8 eV) in contrast with that computed for the BaO monolayer (1.82 eV).

C. Inelastic mean-free path

In general, for a given photon energy, the QE can be increased by reducing the WF. Unfortunately, this also tends to increase the emittance, which is defined as the spread of the emitted electrons in position and momentum. This is because electrons with higher excess energy also have a higher parallel momentum. This has been documented for four MgO layers on Ag(100) where, as the WF decreases by 0.92 eV, the QE and emittance increase relative to the clean Ag(100) surface by a factor of seven and two, respectively. Adapting the photon energy to emit just above threshold could potentially retain the high QE while minimizing the emittance [14]. Traditionally, the light source used in the study of photoemission of metal photocathodes is the third harmonic resonant emission of a Ti:sapphire laser [35]. This light source produces photons with an energy of 4.66 eV which is similar to the WF of metals such as Cu or Ag. The inelastic mean-free path will be increased because electrons with energies close to the Fermi energy will suffer less scattering and so contribute significantly to the QE [36]. Figure 9 shows the computed IMFP of Ag [24]. This suggests a strategy to optimize the QE while minimizing the emittance by designing photocathodes with a low WF and adapting the laser source appropriately.

The WF of an MgO monolayer on Ag(100) calculated in this work is 3.15 eV. For a photon energy of 3.15 eV, the IMFP of the electron increases slightly to 7.65 Å compared with 6.12 Å with a photon energy of 4.7 eV. At 3.15 eV we predict a QE of 5.1×10^{-5} which is only slightly higher than that of the clean Ag(100) surface.

The addition of a BaO monolayer to the Ag(100) surface reduces the WF to 1.82 eV. The IMFP of an electron with an energy of 1.82 eV is estimated to be 11.19 Å, which is nearly twice the IMFP for a photon energy of 4.7 eV. Experimental measurements of BaO monolayers on Ag(100) measured a WF of 2.5 eV. For an electron at this energy the IMFP is estimated to be 8.87 Å. The consequence is that the calculated QE of BaO monolayer on Ag(100) at 1.82 eV is 1.0×10^{-5} and at 2.5 eV is 1.4×10^{-4}. The addition of a BaO monolayer therefore allows the use of a visible light photons instead of conventional UV light sources and at the same time improves significantly the QE of Ag(100).

IV. CONCLUSIONS

The calculations presented here demonstrate that MgO thin films on Ag(100) reduce the work function (WF) by more than 1 eV, in good agreement with previous experimental and theoretical results. The computed quantum efficiency (QE) is maximized for monolayer adsorption and the addition of further layers reduces the QE due to the inelastic scatterings in the oxide film. A layer-by-layer decomposition of the QE shows that the main contribution to the QE is from the layers at the metal-metal oxide interface due to the charge-transfer excitation from the Ag valence band to the MgO conduction band.

The adsorption of BaO thin films reduces the WF of the Ag(100) surface by more than 2 eV. The QE is maximized by the addition of a BaO monolayer and is reduced slightly by the addition of further layers. The layer-by-layer decomposition of a system with four BaO(100) layers on Ag(100) suggests that, for a photon energy of 4.7 eV, electrons are being emitted mainly due to absorption in the BaO thin film. For this system, the QE increased by a factor of 250 for incident photons of 4.7 eV. For the case of MgO on Ag(100) the opportunities for optimization the photoemission is small. The reduction of the WF increases the QE for a photon energy of 4.7 eV but, due to the excess energy, the emittance is also increased. For BaO, the WF reduction means that lower energy visible photons can be used to enhance the emission of electrons. In addition, by lowering the incident photon energy, only low parallel momentum electrons will be emitted and this will also reduce the emittance while retaining a reasonable QE, due to the increment of the mean-free path of low-energy electrons.

ACKNOWLEDGMENTS

The authors would like to thank M. Surman and E. A. Seddon for the useful discussions. This work made use of the high-performance computing facilities of Imperial College London. The project is carried out in collaboration with the ASTeC group based at the Daresbury Laboratories and is funded by the Science and Technology Facilities Council. V.C. was supported by the EPSRC Centre for Doctoral Training in Advance Characterisation of Materials (Grant No. EP/L015277/1).

[1] C. Pellegrini, Eur. Phys. J. H **37**, 659 (2012).
[2] B. W. J. McNeil and N. R. Thompson, Nat. Photonics **4**, 814 (2010).
[3] D. H. Dowell, I. Bazarov, B. Dunham, K. Harkay, C. Hernandez-Garcia, R. Legg, H. Padmore, T. Rao, J. Smedley, and W. Wan, Nucl. Instrum. Methods Phys. Res., Sect. A **622**, 685 (2010).
[4] B. Camino, T. C. Q. Noakes, M. Surman, E. A. Seddon, and N. M. Harrison, Comput. Mater. Sci. **122**, 331 (2016).
[5] F. J. Himpsel and D. Eastman, J. Vac. Sci. Technol. **16**, 1297 (1979).
[6] N. Lopez and S. Valeri, Phys. Rev. B **70**, 125428 (2004).
[7] T. Jaouen, G. Jźquel, G. Delhaye, B. Pine, P. Turban, and P. Schieffer, Appl. Phys. Lett. **97**, 232104 (2010).
[8] H. J. Freund and G. Pacchioni, Chem. Soc. Rev. **37**, 2224 (2008).
[9] S. Prada, U. Martinez, and G. Pacchioni, Phys. Rev. B **78**, 235423 (2008).
[10] J. Goniakowski and C. Noguera, Phys. Rev. B **79**, 155433 (2009).
[11] T. Konig, G. H. Simon, H.-P. Rust, and M. Heyde, J. Phys. Chem. C **113**, 11301 (2009).
[12] K. Németh, K. C. Harkay, M. van Veenendaal, L. Spentzouris, M. White, K. Attenkofer, and G. Srajer, Phys. Rev. Lett. **104**, 046801 (2010).
[13] L. Giordano, F. Cinquini, and G. Pacchioni, Phys. Rev. B **73**, 045414 (2006).
[14] T. C. Droubay, S. A. Chambers, A. G. Joly, W. P. Hess, K. Németh, K. C. Harkay, and L. Spentzouris, Phys. Rev. Lett. **112**, 067601 (2014).
[15] J. A. Assimos and D. Trivich, Phys. Status Solidi A **26**, 477 (1974).
[16] S. J. Clark, M. D. Segall, C. J. Pickard, P. J. Hasnip, M. I. J. Probert, K. Refson, and M. C. Payne, Z. Kristallogr. **220**, 567 (2005).
[17] J. P. Perdew, A. Ruzsinszky, G. I. Csonka, O. A. Vydrov, G. E. Scuseria, L. A. Constantin, X. Zhou, and K. Burke, Phys. Rev. Lett. **100**, 136406 (2008).
[18] J. D. Pack and H. J. Monkhorst, Phys. Rev. B **16**, 1748 (1977).
[19] L. G. Liu and W. A. Bassett, J. Appl. Phys. **44**, 1475 (1973).
[20] R. M. Hazen, Am. Mineral. **61**, 266 (1976).
[21] R. J. Zollweg, Phys. Rev. **100**, 671 (1955).
[22] J. Wang and S. Q. Wang, Surf. Sci. **630**, 216 (2014).
[23] C. N. Berglund and W. E. Spicer, Phys. Rev. **136**, A1030 (1964).
[24] I. Nagy and P. M. Echenique, Phys. Rev. B **85**, 115131 (2012).
[25] H. T. Nguyen-Truong, J. Phys.: Condens. Matter **29** 215501 (2017).
[26] S. Benedetti, N. Nilius, P. Torelli, G. Renaud, H. J. Freund, and S. Valeri, J. Phys. Chem. C **115**, 23043 (2011).
[27] H. B. Michaelson, J. Appl. Phys. **48**, 4729 (1977).
[28] D. Velázquez, R. Seibert, H. Ganegoda, D. Olive, A. Rice, K. Logan, Z. Yusof, L. Spentzouris, and J. Terry, Appl. Surf. Sci. **360**, 762 (2016).
[29] S. Prada, L. Giordano, G. Pacchioni, and J. Goniakowski, Appl. Surf. Sci. **390**, 578 (2016).
[30] T. C. Droubay, L. Kong, S. A. Chambers, and W. P. Hess, Surf. Sci. **632**, 201 (2015).
[31] J. L. Jord and T. K. Jondo, J. Alloys Compd. **327**, 167 (2001).
[32] S. C. Middleburgh, K. P. D. Lagerlof, and R. W. Grimes, J. Am. Ceram. Soc. **96**, 308 (2013).
[33] A. Apker, E. Taft, and J. Dickey, Phys. Rev. **84**, 508 (1951).
[34] E. B. Hensley and George A. Saum, Phys. Rev. **113**, 1019 (1959).
[35] P. F. Moulton, J. Opt. Soc. Am. B **3**, 125 (1986).
[36] B. Ziaja, R. A. London, and J. Hajdu, J. Appl. Phys. **99** 033514 (2006).